ACS APPLIED MATERIALS & INTERFACES
Research Article
www.acsami.org

Impact of Al Passivation and Cosputter on the Structural Property of β-$FeSi_2$ for Al-Doped β-$FeSi_2$/n-Si(100) Based Solar Cells Application

Goutam Kumar Dalapati,*[†] Avishek Kumar,[†,‡,§] Cheng Cheh Tan,[†] Siao Li Liew,[†] Prashant Sonar, Hwee Leng Seng, Hui Kim Hui,[†] Sudhiranjan Tripathy,[†] and Dongzhi Chi[†]

[†]Institute of Materials Research and Engineering, A*STAR (Agency for Science, Technology and Research), 3 Research Link, Singapore 117602

[‡]Solar Energy Research Institute of Singapore, National University of Singapore, Singapore 117574

[§]Department of Electrical and Computer Engineering, National University of Singapore, Singapore 117583

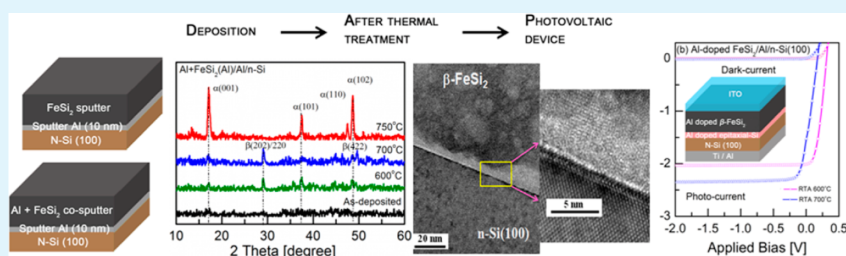

ABSTRACT: The aluminum (Al) doped polycrystalline *p*-type β-phase iron disilicide (*p*-β-$FeSi_2$) is grown by thermal diffusion of Al from Al-passivated *n*-type Si(100) surface into $FeSi_2$ during crystallization of amorphous $FeSi_2$ to form a *p*-type β-$FeSi_2$/*n*-Si(100) heterostructure solar cell. The structural and photovoltaic properties of *p*-type β-$FeSi_2$/*n*-type c-Si structures is then investigated in detail by using X-ray diffraction, Raman spectroscopy, transmission electron microscopy analysis, and electrical characterization. The results are compared with Al-doped *p*-β-$FeSi_2$ prepared by using cosputtering of Al and $FeSi_2$ layers on Al-passivated *n*-Si(100) substrates. A significant improvement in the maximum open-circuit voltage (V_{oc}) from 120 to 320 mV is achieved upon the introduction of Al doping through cosputtering of Al and amorphous $FeSi_2$ layer. The improvement in V_{oc} is attributed to better structural quality of Al-doped $FeSi_2$ film through Al doping and to the formation of high quality crystalline interface between Al-doped β-$FeSi_2$ and *n*-type c-Si. The effects of Al-out diffusion on the performance of heterostructure solar cells have been investigated and discussed in detail.

KEYWORDS: *doped β-$FeSi_2$, Al-passivation, rapid-thermal-annealing, Al out-diffusion, Raman spectroscopy, photovoltaic*

1. INTRODUCTION

The semiconducting beta-phase of iron disilicide (β-$FeSi_2$) has attracted considerable attention due to its potential applications in optoelectronic and microelectronic areas.[1] β-$FeSi_2$ has a high optical absorption coefficient (>10^5 cm^{-1} at 1.0 eV), which is 200-fold larger than that of crystalline silicon, and a direct optical band gap of 0.85 eV.[1−3,5] In addition, β-$FeSi_2$ is an earth-abundant, nontoxic material compatible with silicon technology which makes it a desirable candidate for novel photovoltaic applications,[4] with a theoretical energy conversion efficiency up to 23%.[4,10] However, only a limited number of experimental results on β-$FeSi_2$ solar cells exist to date.[6−9] Most of the results are reported on solar cells fabricated using undoped β-$FeSi_2$ thin films grown on crystalline silicon (c-Si) wafers. Undoped β-$FeSi_2$ films exhibit *n*-type or *p*-type characteristics based on their fabrication techniques.[1,6] The highest reported efficiency to date is only 3.7% for epitaxially grown undoped β-$FeSi_2$ (*n*-type)/*p*-type c-Si heterojunction solar cells prepared by facing-target sputtering (FTS) method using a dedicated system and a complex process with several intermediate steps.[6] Recently, we have introduced a relatively less complex process to fabricate β-$FeSi_2$ thin films using conventional magnetron sputtering and rapid thermal processing.[11,12] Al-doped *p*-type β-$FeSi_2$ thin films were deposited on *n*-type c-Si wafer to fabricate a *p*-type β-$FeSi_2$/*n*-type c-Si heterojunction solar cells. The performance of the fabricated heterojuncton solar cell was very poor due to the formation of a thin amorphous layer at the *p*-β-$FeSi_2$/*n*-Si interface.[12] The performance of the heterostructure was drastically improved with Al interface engineering.[12] The Al interlayer deposited between the β-$FeSi_2$ and c-Si layers, reacts with Si in $FeSi_2$ during the thermal processing step to produce a high quality crystalline interface between β-$FeSi_2$ and *n*-type c-Si through the formation of a thin, highly Al-doped epitaxial Si (p^+ Si) interfacial layer.[12] From the reported results, it is almost certain that the Al interlayer plays a key role to integrate β-phase $FeSi_2$ with Si. However, not much was reported over the role of the Al dopant, out diffusion of Al from the Al interlayer, and how it

Received: January 31, 2013
Accepted: June 4, 2013
Published: June 4, 2013

 © 2013 American Chemical Society

would affect the structural and electrical properties of the *p*-type β-$FeSi_2$/n-type c-Si heterostructure solar cells. There is limited work on the Al-dopant and diffusion of Al dopant in β-$FeSi_2$ with the few exception of the study by Liu et al., where they studied the effect of thermal treatment on Al out diffusion in an Al doped β-$FeSi_2$ thin film prepared by molecular beam epitaxy.[13] Formation of *p*-type β-$FeSi_2$ using the method of thermal diffusion of an evaporated Al dopant layer was also reported by Momose et al.;[8] however, nothing much was reported about the structure and quality of the film. It is very important to note that the crystal structure and doping density of the layer depends on the thermal treatment and out diffusion of Al.

In the present work, we have investigated the impact of Al passivation and Al cosputter on the structural quality of $FeSi_2$ thin films. The structural property of the $FeSi_2$ and Al-doped $FeSi_2$ film was investigated by using X-ray diffraction (XRD) and Raman spectroscopy. Interface quality at $FeSi_2$/*n*-Si(100) and Al diffusion were studied in detail by using secondary ion mass spectroscopy (SIMS) and high-resolution transmission electron microscopy (HRTEM) analysis. Photovoltaic characteristics of β-$FeSi_2$ and Al-doped β-$FeSi_2$ films on Al (~10 nm thin) passivated *n*-type c-Si(100) were investigated.

2. EXPERIMENTAL SECTION

Thin films of β-$FeSi_2$ were grown on *n*-Si(100) substrates. The substrates were dipped into diluted hydrofluoric acid solution (1%) to remove the native oxide. After cleaning, the substrates were immediately loaded into a magnetron sputtering chamber with a base pressure of 2×10^{-7} Torr. A layer of ~60 nm thick amorphous $FeSi_2$ was deposited at room temperature by using stoichiometric $FeSi_2$ target in Ar ambient at a working pressure of 3 mTorr. Prior to the deposition of amorphous-$FeSi_2$, ~10 nm thin Al interlayer was deposited. The samples were then subjected to rapid-thermal-annealing (RTA) in nitrogen ambient at temperatures of 600−750 °C for 60 s. For some wafers, Al-doped $FeSi_2$ was grown by using cosputter of $FeSi_2$ and pure Al targets on (~10 nm thin) Al-passivated *n*-Si(100) substrates. The formation of polycrystalline β-phase was confirmed by X-ray diffraction (XRD) and Raman spectroscopy. The Al-depth profile after RTA was investigated using SIMS analysis. The film thickness, microstructure, composition, and interfacial layers were examined by high-resolution transmission electron microscopy (HRTEM) and energy dispersive X-ray spectroscopy analysis. Photoelectron spectroscopy in air (PESA) measurement was done on the $FeSi_2$/Al/n-Si substrate using Riken photoelectron spectrometer (model AC-2). Finally, a 200 nm thick indium−tin-oxide (ITO) was deposited at room temperature on $FeSi_2$ film as a top electrode and at thin film of Ti/Al alloy was sputter deposited on the back side of *n*-Si to achieve a low resistance Ohmic contact. Figure 1 shows the schematic diagram of steps involved in the fabrication of the β-$FeSi_2$ and Al-doped β-$FeSi_2$ heterojunction solar cells grown on Al-passivated *n*-Si(100) substrates. The Photovoltaic properties of the ITO/*p*-β-$FeSi_2$/*n*-Si(100) and ITO/Al-doped *p*-β-$FeSi_2$/*n*-Si(100) heterojunction solar cells were measured under standard AM 1.5 illumination.

3. RESULTS AND DISCUSSION

Figure 2 shows the XRD spectrum of $FeSi_2$ and Al-doped $FeSi_2$ films for different RTA temperatures. No diffraction peaks are observed for the as-deposited film, indicating an amorphous nature of the films. A sharp distinct peak at 28.5° is observed for sample annealed at 600−700 °C corresponding to (202/220) planes of β-$FeSi_2$.[14] Few other low intensity peaks are also observed which can be attributed to a possible (*hkl*) orientations, as indicated in the figure, confirming the

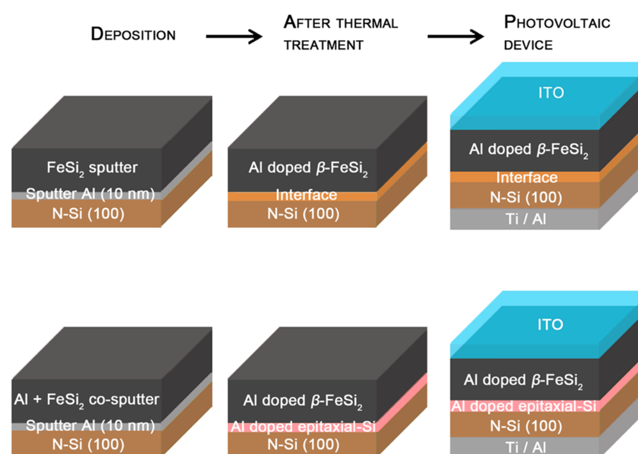

Figure 1. Schematic diagram of $FeSi_2$ and Al-doped $FeSi_2$ films on Al-passivated *n*-Si(100) substrates.

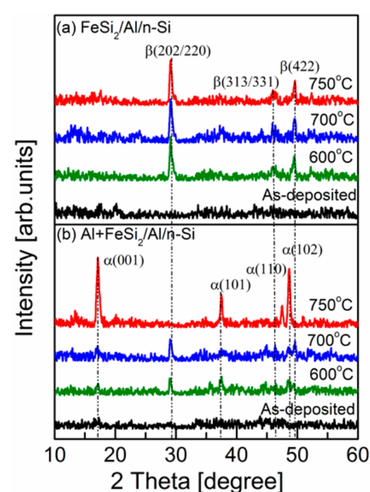

Figure 2. (a) XRD spectra of as-deposited and annealed $FeSi_2$/Al/*n*-Si(100) heterostructure under glancing angle incidence configuration ($\Omega = 2°$). (b) XRD spectra of as-deposited and annealed Al-doped $FeSi_2$/Al/*n*-Si (100) heterostructure. The annealing temperature is indicated in the figure.

formation of polycrystalline orthorhombic β-$FeSi_2$[14] for the samples annealed between 600 and 700 °C. $FeSi_2$/Al/*n*-Si(100) samples behaved differently when compared to Al-doped $FeSi_2$/Al/*n*-Si(100) samples after annealed at 750 °C, as shown in Figures 2a and b, respectively. While no significant difference in XRD pattern is observed for $FeSi_2$/Al/*n*-Si(100) samples annealed at 750 °C, the Al-doped $FeSi_2$/Al/*n*-Si(100) samples shows a phase transformation from the orthorhombic β-phase to alpha (α) phase at 750 °C, as can be seen in Figure 2b. Zhang and Saxena[15] reported phase transformation of $FeSi_2$ film from β to α at high temperature. In the present work, we observed α-phase in Al-doped $FeSi_2$ at a significantly low temperature of 750 °C indicating that the Al concentration in $FeSi_2$ film influences the phase transformation at low temperature. The samples were further analyzed in detail using Raman spectroscopy to understand the impact of RTA and Al doping on the crystal quality of $FeSi_2$ and Al-doped $FeSi_2$ films.

Figure 3a and b shows the Raman spectra recorded from the $FeSi_2$/Al/*n*-Si(100) and Al-doped $FeSi_2$/Al/*n*-Si(100) structures, respectively, for the as-deposited and different RTA

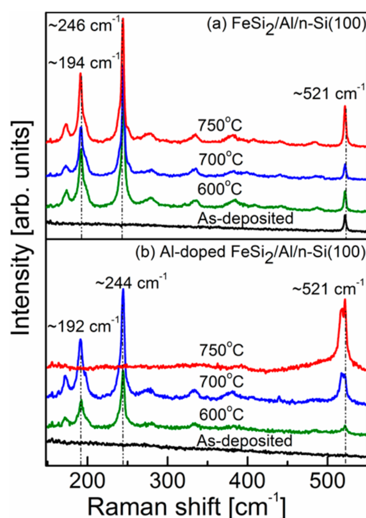

Figure 3. (a) Raman spectra of as-deposited and annealed $FeSi_2$/Al/*n*-Si(100) heterostructure. (b) Raman spectra of as-deposited and annealed Al-doped $FeSi_2$/Al/*n*-Si(100) heterostructure. The annealing temperature is indicated in the figure.

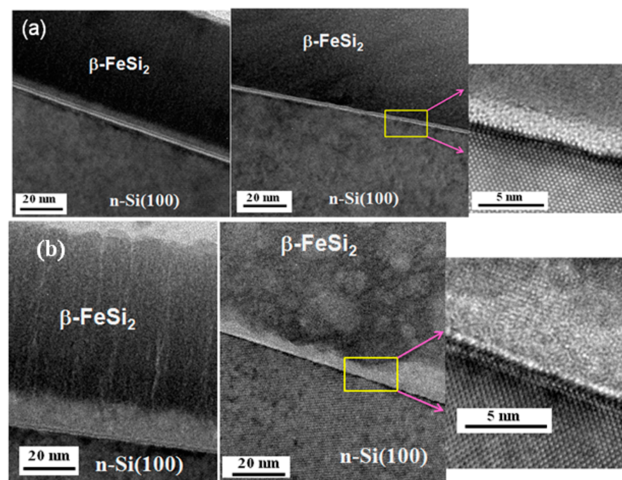

Figure 4. (a) Cross-sectional image of $FeSi_2$/Al/*n*-Si(100) heterostructure and the HRTEM image $FeSi_2$/Al/*n*-Si interface after RTA at 600 °C. (b) Cross-sectional TEM image of Al-doped $FeSi_2$/Al/*n*-Si heterostructure and the HRTEM image Al-doped $FeSi_2$/Al/*n*-Si interface after RTA at 600 °C.

temperature conditions. Raman spectra were acquired using a Jobin Yvon LABRAM system equipped with a 488 nm laser line. For the as-deposited $FeSi_2$/Al/*n*-Si(100) samples, a Raman peak at 521 cm^{-1} corresponding to bulk Si substrate O(Γ) phonon is observed while no clear Raman lines related to crystalline phase of Fe−Si can be seen, thus indicating the amorphous nature of $FeSi_2$. Two distinct peaks centered at ∼194 and ∼246 cm^{-1} tend to appear for samples annealed between 600 and 700 °C confirming the formation of the β phase in the $FeSi_2$ layer.[16,18] The intensity of the optical phonon peak from bulk Si substrate shows a gradual increase with increasing annealing temperature to 750 °C. This confirms the improvement of transmittance of the film due to probing with a visible laser line and could be related to an increase in crystalline ordering at higher annealing temperature. However, Al-doped $FeSi_2$/Al/*n*-Si(100) samples show a slightly different trend with no noticeable peak from the as-deposited samples. The samples annealed between 600 and 700 °C showed a slight shift in the frequency with the peak indexed at ∼192 and ∼244 cm^{-1} respectively. The absence of the peak at 521 cm^{-1} for the as-deposited Al-doped $FeSi_2$/Al/*n*-Si(100) samples could be due to the influence of a heavy concentration of Al atoms in the amorphous phase layers and leading to a shallow probing depth of 488 nm excitation line. However, the sharp distinct Raman peak at 521 cm^{-1} from Si substrate began to appear for samples annealed at ≥600 °C indicating the improvement in crystalline nature of the layers. Furthermore, we clearly observed Raman peak around 515−517 cm^{-1} in the spectra from such annealed layers due to the formation of microcrystalline Si phase at the interfaces through Al induced crystallization of amorphous $FeSi_2$. This is also complimented by a low energy line shape asymmetry associated with a broader peak from mixed amorphous-nano silicon phases at substrate interfaces. The slight frequency shift observed in the Raman line for Al-doped $FeSi_2$/Al/*n*-Si(100) samples annealed between 600 and 700 °C could be attributed to the improvement in the crystalline alloy phase due high Al contents.[19] The improvement in the structural quality of the Al-doped $FeSi_2$/Al/*n*-Si(100) with respect to undoped $FeSi_2$/Al/*n*-Si(100) were also confirmed from the TEM images (Figure 4). The improvement in structural and electrical properties of β-$FeSi_2$ with the incorporation of Al is also observed by other groups.[18−20] Furthermore, a detailed analysis of the Raman spectra reveals additional broad features at ∼280, ∼335, and ∼380 cm^{-1} for $FeSi_2$/Al/*n*-Si(100) samples annealed between 600 and 700 °C and Al-doped $FeSi_2$/Al/*n*-Si(100) samples annealed at 700 °C, respectively. These broad features can be attributed to the disorder-induced Raman scattering from the presence of the lattice imperfection on the nonstoichiometric β phase,[19,23] possibly due to the varying distribution of the Al dopant into the β-$FeSi_2$ films as a function of different RTA temperatures. The Raman peak at ∼192 and ∼244 cm^{-1} disappears for Al-doped $FeSi_2$/Al/*n*-Si(100) samples annealed at 750 °C, indicating the transformation of β-$FeSi_2$ to α phase whereas as no noticeable difference is observed for $FeSi_2$/Al/*n*-Si(100) samples annealed at 750 °C. The Raman results are in good agreement with the XRD spectrum (Figure 2).

Figure 4 shows the cross-sectional TEM and HRTEM images for $FeSi_2$/Al/*n*-Si(100) structure and Al-doped $FeSi_2$/Al/*n*-Si(100) structure, for as-deposited and annealed at 700 °C. According to the TEM images, the thicknesses of Al-passivation layer and $FeSi_2$ layer are ∼7 and 57 nm, respectively for the as-deposited sample. Al-passivation layer thickness is ∼12 nm and total thickness is 78 nm for Al-doped $FeSi_2$/Al/*n*-Si(100) structure. There is a presence of thin amorphous layer of SiO_2 for both the cases. The HRTEM image reveals a distortion at the $FeSi_2$/*n*-Si interface with the presence of thick amorphous layer after annealing at 700 °C of $FeSi_2$/Al/*n*-Si(100) structure as shown in Figure 4a. On the other hand, a sharp interface is observed between $FeSi_2$ and *n*-Si for Al-doped $FeSi_2$/Al/*n*-Si(100) structure (Figure 4b). The thickness of amorphous layer is also reduced through the formation of regrown Si layer. The formation of amorphous $SiAl_xFe_yO_z$ layer is mainly due to the presence of residual oxygen during sputter and thermal treatment of $FeSi_2$ layer. The Al passivation layer was mostly dissolved into $FeSi_2$ layer to replace Si, as a result formation of heavily Al-doped regrown-Si interfacial layer is observed at Al-doped $FeSi_2$/*n*-Si interface. It is worth to note that the formation of regrown Si layer is depend on the crystallization temperature of $FeSi_2$ layer, thickness of Al passivation layer, and

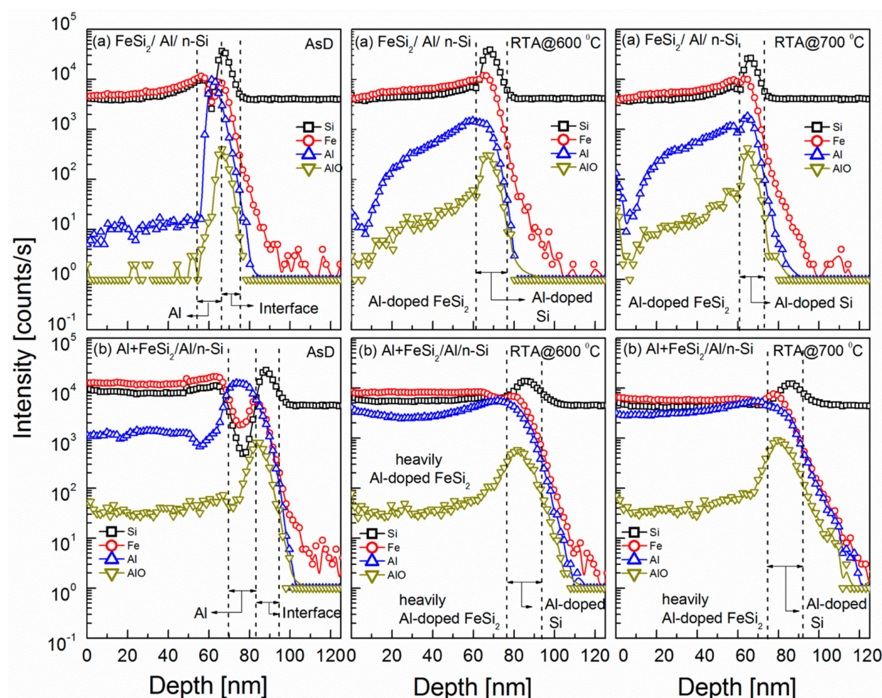

Figure 5. SIMS depth profile for Al, Fe, Si and AlO measured on (a) as-deposited and annealed $FeSi_2$/Al/*n*-Si(100) heterostructures and (b) as-deposited and annealed Al-doped $FeSi_2$/Al/*n*-Si heterostructures.

thickness of $FeSi_2$ layer.[12,18] The significance and impact of Al concentration on the β-$FeSi_2$/Si interface has also been discussed in detail by Kumar et al.,[18] where the interface quality tended to decease with the decrease in the ratio of the Al concentration to $FeSi_2$ film thickness.

Furthermore, SIMS analysis was conducted to evaluate the Al distribution in the β-$FeSi_2$ films. Figure 5a shows the SIMS depth profile of $FeSi_2$/Al/*n*-Si(100) structure, and Figure 5b shows the Al-doped $FeSi_2$/Al/*n*-Si(100) structure. It is quite evident from the SIMS result that, Fe and Si were uniformly distributed in the $FeSi_2$ layer and there is a highly Al doped regrown Si interlayer between the Si and $FeSi_2$ films for al samples annealed at ≥600 °C. A ~10 nm of Al interlayer can be clearly observed for the as-deposited samples which react with $FeSi_2$ at high temperature to form an Al-doped epitaxial Si interfacial layer, as is evident in Figure 5, for samples annealed at ≥600 °C. It is interesting to note that SIMS intensity for Si at the interface is marginally higher than that of $FeSi_2$ film and the subsequent c-Si substrate. At interface, the intensity of Si signal is due to the contribution of from both, crystalline Si, and the interface Si (SiO_2 or regrown Si). The high intensity of Si is mainly due to the Si signal from c-Si and the interfacial SiO_2 layer for the as-deposited films, and regrown Si layer for annealed samples. The height and width of Si peak changes with the variation of annealing temperature and nature of samples, which suggest the formation of regrown Si layer during thermal treatment of $FeSi_2$ layer.

Further analysis of SIMS reveals that as expected, the Al concentration in the as-deposited $FeSi_2$/Al/*n*-Si(100) structure is negligible (Figure 5a) while a uniform Al concentration can be seen in the $FeSi_2$ film for the as-deposited Al-doped $FeSi_2$/Al/*n*-Si(100) structure (Figure 5b). Al from the Al interlayer diffuses through the $FeSi_2$ film resulting in the increase of Al concentration in the $FeSi_2$ films for the samples annealed at 600 °C and above (Figure 5). From Figure 5a, it is also revealed that the RTA temperature of 600 °C is enough to create a *p*-type β-$FeSi_2$ film due to the Al diffusion from the interlayer for $FeSi_2$/Al/*n*-Si(100) structure. It is interesting to note that the Al diffusion profile is significantly different for the Al-doped $FeSi_2$/Al/*n*-Si(100) structure. A two-way Al diffusion profile as a function of annealing temperature can be clearly seen. The Al concentration in the $FeSi_2$ film increases with the increase in the annealing temperature. The significant amount of Al also diffuses into Si substrates at the annealing temperature of 700 °C.

To further evaluate the significance of Al doping in the $FeSi_2$ and its impact on the performance of the heterojunction solar cells, the ITO/$FeSi_2$/*n*-Si(100) and ITO/Al-doped $FeSi_2$/*n*-Si(100) heterostructures were evaluated through current voltage measurements. A typical *p*-*n* type characteristic can been seen for both the structure annealed at ≥600 °C which is in good agreement with the SIMS results indicating the *p*-type conductivity of β-$FeSi_2$ in $FeSi_2$/*n*-Si(100) and Al-doped $FeSi_2$/*n*-Si(100) structure, respectively. Figure 6 shows the dark current density comparison for the ITO/$FeSi_2$/*n*-Si(100) and ITO/Al-doped $FeSi_2$/*n*-Si(100) structure. For the undoped $FeSi_2$ films, the dark current density decreases with the increase of annealing temperature. On the other hand, for Al-doped $FeSi_2$ films, the dark current density increases significantly after annealing at 700 °C. Therefore, it is worth to note that the introduction of Al doping into $FeSi_2$ using different methods has significant role on the formation of *p*-*n* junction as well as crystal quality of $FeSi_2$. By using cosputter of Al, it is possible to achieve high quality *p*-*n* junction with low dark current density even at 600 °C. At high temperature, there is a slight increase of the dark current density due to the degradation of interface quality. In our previous work, we have observed the sharp crystalline interface between *n*-Si(100) and $FeSi_2$ at a temperature of 650 °C through the formation of regrown epitaxial Si.[12] In the present work, according to TEM images,

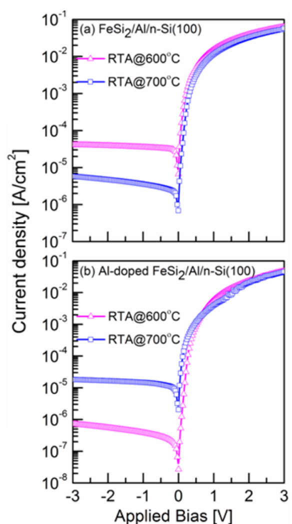

Figure 6. Dark current density comparison in logarithm scale between (a) $FeSi_2$/Al/*n*-Si heterostructures annealed at 600−700 °C and (b) Al-doped $FeSi_2$/Al/*n*-Si heterostructures annealed at 600−700 °C.

the interface is not very sharp. Even though, there is a presence of regrown epitaxial-Si at the interface, the regrown Si is not uniform. On the other hand, for undoped $FeSi_2$, we need high temperature to achieve low dark current. For undoped $FeSi_2$, with the increase of annealing temperature, Al dopant diffuse into $FeSi_2$ more uniformly, improved crystalline quality of the film.

Figure 7a and b shows the current density−voltage (J−V) characteristics of the ITO/$FeSi_2$/*n*-Si(100) and ITO/Al-doped

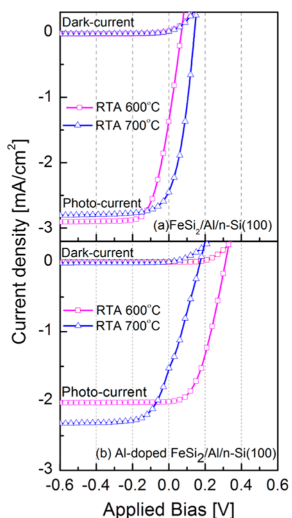

Figure 7. Current−voltage (J−V) characteristics of (a) $FeSi_2$/Al/*n*-Si and (b) Al-doped $FeSi_2$/Al/*n*-Si heterojunction solar cells (device size; 2.5 × 2.5 mm^2) in dark and under light of air mass 1.5 and 100 mW/cm^2 illumination.

$FeSi_2$/*n*-Si(100) heterostructures solar cells devices, respectively. It can be clearly observed that the V_{oc} of the Al-doped $FeSi_2$/*n*-Si(100) heterostructure solar cell is significantly higher than that of undoped $FeSi_2$/*n*-Si(100) heterojunction while both have similar low J_{sc}, resulting in a better performance of the solar cell. The possible reason for the better performance of the Al-doped $FeSi_2$/*n*-Si(100) solar cells could be that Al doped samples had sufficient Al concentration to produce a sharp and better quality interface between β-$FeSi_2$/*n*-Si through the formation of regrown Si layer at the interface. In addition, an increase in the Al concentration in the $FeSi_2$ film helps to reduce the voids in the $FeSi_2$ film which makes the surface smooth and thus improves the performance of the solar cell by reducing the defect states.[22] It is also interesting to note that the best performance of the $FeSi_2$/*n*-Si(100) heterojunction solar cell was achieved for the samples annealed at 700 °C while that the best performance of the Al-doped $FeSi_2$/*n*-Si(100) heterojunction solar cell was achieved for the samples annealed at 600 °C. As the $FeSi_2$ film in $FeSi_2$/Al/*n*-Si(100) structure is undoped, this observation could be a result of the Al diffusing through the film from the Al interlayer during the annealing of the sample. Hence, the Al concentration in the $FeSi_2$ film would increase as the annealing temperature increased from 600 to 700 °C as is evident from SIMS results (Figure 5a). This would lead to the improvement of the $FeSi_2$ film as also observed from the Raman measurements (Figure 3a). In comparison, for Al-doped $FeSi_2$/Al/*n*-Si(100) structures, a dual diffusion mechanism occurs as Al from the interlayer diffuses into the $FeSi_2$ film as well as into *n*-Si(100) substrates. Furthermore, there is an interdiffusion of Al present in the $FeSi_2$ film. Thus, with the increase of annealing temperature from 600 to 700 °C, Al out diffuses from the $FeSi_2$ film and the Al interlayer into the *n*-Si(100), which also might be the key factor for degradation of the Al-doped $FeSi_2$/*n*-Si(100) device at 700 °C. In addition, a higher annealing temperature could lead to the formation of pinholes in the β-$FeSi_2$ film,[24] which could add up to deteriorate the performance of the solar cells which is quite evident from the sharp decrease in the V_{oc} from 320 to 180 mV on the increase of annealing temperature from 600 to 700 °C.

The solar cell parameters of the four selected heterostructure solar cell samples are summarized in Table 1. It is quite evident that the Al-doped $FeSi_2$/Al/n-Si(100) heterostructure annealed at 600 ^{o}C is the best solar cell. The efficiency of the device is lower than the reported results by Liew et al.,[11] due to the variation of Al concentration in the $FeSi_2$ films. It is worth noting that the efficiency of the device depends on Al concentration as well as thickness of the $FeSi_2$ layer. There is a significant impact of the Al on the performance of the solar cell device, particularly, open circuit voltage and fill factor. The fill factor (FF) for the device using undoped $FeSi_2$ is improved from ∼20% to 41% after annealing at 700 °C, suggesting improved contact resistance between $FeSi_2$ and ITO, through the uniform distribution of Al in $FeSi_2$ film. On the other hand, for Al-doped $FeSi_2$, the FF of the device degrades significantly with the increase of annealing temperature. This is due to the poor contact between ITO and Al-doped $FeSi_2$. The work function of sputter deposited ITO is ∼4.3 eV.[25] From the photoelectron spectrum of the undoped β-$FeSi_2$ film, the ionization potential (work function) was determined and the value is ∼5.2 eV, as shown in Figure 8, and it varies with Al concentration. By minimizing the work function difference between ITO and β-$FeSi_2$, it is possible to improve the contact resistance of ITO/*p*-type β-$FeSi_2$. Recently, it was shown by Lee et al.[26] that the performance of silicone heterojunction solar cells closely correlated with the work function difference between silicon and transparent conducting oxide. Thus performance of the β-$FeSi_2$ based solar cell can be better through the improvement of *FF*. Even though efficiency of the device is not high, the present research shows feasibility of cosputter, Al diffusion, and thermal treatment of $FeSi_2$ to form β-phase and α phase $FeSi_2$ at low temperature.

Table 1. Solar Cell Parameters of $FeSi_2$/Al/*n*-Si(100) and Al-Doped $FeSi_2$/Al/*n*-Si(100) Heterostructure Annealed at 600 and 700 °C, Respectively, over the AM 1.5 G Solar Spectra[a]

solar cell samples	J_{sc} [mA/cm^2]	V_{oc} [mV]	FF [%]	eff [%]
$FeSi_2$/Al/n-Si(100) RTA@600 °C	2.01	60	20.7	0.025
$FeSi_2$/Al/n-Si(100) RTA@700 °C	2.45	120	41.8	0.123
Al-doped $FeSi_2$/Al/n-Si(100) RTA@600 °C	2.01	320	43.5	0.28
Al-doped $FeSi_2$/Al/n-Si(100) RTA@700 °C	1.53	180	26.1	0.072

[a]All cells have an area of 2.5 × 2.5 mm^2.

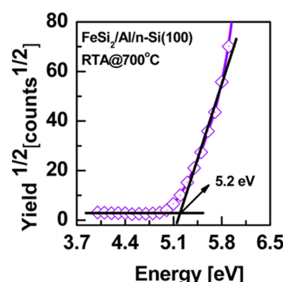

Figure 8. Photoelectron spectrum of $FeSi_2$/Al/*n*-Si(100) structure after annealed at 700 °C.

4. CONCLUSION

In conclusion, we successfully fabricated *p*-*β*-$FeSi_2$ using thermal diffusion of Al from Al-passivated *n*-Si(100) surface into $FeSi_2$ during crystallization of amorphous $FeSi_2$; and we compared the resultant device with Al-doped p-type *p*-*β*-$FeSi_2$ by using cosputtered of Al and amorphous $FeSi_2$ layers on Al-passivated *n*-Si(100) substrates. The experimental results highlighted that even though diffusion of Al from Al-passivated Si surface into $FeSi_2$ was sufficient to change the polarity of *β*-$FeSi_2$ to *p*-type for a *p*-*n* junction with *n*-Si(100), the material quality was significantly compromised, resulting in the poor performance of the solar cell as compared to Al-doped $FeSi_2$/Al/*n*-Si heterojunction solar cells. A significant improvement in the maximum V_{oc} from 120 to 320 mV was observed upon the introduction of Al doping achieved through cosputtering of Al and amorphous $FeSi_2$ layers. Reduction of interfacial layer thickness and formation of regrown Si layers are mainly responsible for the better performance of the device. The improvement in the V_{oc} can be mainly attributed to the $FeSi_2$ layer in the $FeSi_2$/*n*-Si interface, material quality, and the improvement of the doping concentration in $FeSi_2$ films.

■ AUTHOR INFORMATION

Corresponding Author

*E-mail: dalapatig@imre.a-star.edu.sg.

Notes

The authors declare no competing financial interest.

■ REFERENCES

(1) Leong, D.; Harry, M.; Reeson, K. J.; Homewood, K. P. *Nature* **1997**, *387*, 686−688.
(2) Yamaguchi, K.; Mizushima, K. *Phys. Rev. Lett.* **2011**, *86*, 6006−6009.
(3) Noda, K.; Terai, Y.; Hashimoto, S.; Yoneda, K.; Fujiwara, Y. *Appl. Phys. Lett.* **2009**, *94*, 241907.
(4) Makita, Y.; Ootsuka, T.; Fukuzawa, Y.; Otogawa, N.; Abe, H.; Zhengxin, L.; Nakayama, Y. *Proc. SPIE* **2006**, *6197*, 61970O.
(5) Suemasu, T.; Takakura, K.; Li, C.; Ozawa, Y.; Kumagi, Y.; Hasegawa, F. *Thin Solid Films* **2004**, *461*, 209−218.
(6) Liu, Z.; Wang, S.; Otogawa, N.; Suzuki, Y.; Osamura, M.; Fukuzawa, Y.; Ootsuka, T.; Nakamaya, Y.; Tanoue, H.; Makita, Y. *Sol. Energy Mater. Sol. Cells* **2006**, *90*, 276−282.
(7) Shaban, M.; Nakashima, K.; Yokoyama, W.; Yoshitake, T. *Jpn. J. Appl. Phys.* **2007**, *46*, L667−L669.
(8) Momose, N.; Shirai, J.; Tahara, H.; Todoroki, Y.; Hara, T.; Hashimoto, Y. *Thin Solid Films* **2007**, *515*, 8210−8215.
(9) Liu, Z.; Watanabe, M.; Hanabusa, M. *Thin Solid Films* **2001**, *381*, 262−269.
(10) Libezny, M.; Poortmans, J.; Vermeulen, T.; Nijs, J.; Amesz, P. H.; Herz, K.; Powalla, M.; Reinsperger, G. U.; Schmidt, M.; Hoffmann, V.; Lange, H. *Proc. 13th Eur. Photovoltaic Sol. Energy Conf.* **1995**, 1326.
(11) Liew, S. L.; Chai, Y.; Tan, H. R.; Hui, H. K.; Wong, A. S.W.; Dalapati, G. K.; Chi, D. Z. *J. Electrochem. Soc.* **2012**, *159*, H52−H56.
(12) Dalapati, G. K.; Liew, S. L.; Wong, A. S. W.; Chai, Y.; Chiam, S. Y.; Chi, D. Z. *Appl. Phys. Lett.* **2011**, *98*, 013507.
(13) Liu, Z.; Kurodo, R.; Fukuzawa, Y.; Makita, Y.; Tanoue, H. *Appl. Phys. Express* **2008**, *1*, 101402.
(14) Tan, D.; Chua, C. T.; Dalapati, G. K.; Chi, D. Z. *Thin Solid Films* **2012**, *520*, 2336−2338.
(15) Zhang, F. X.; Saxena, S. *Scr. Mater.* **2006**, *54*, 1375−1377.
(16) Batalov, R. I.; Bayazitov, R. M.; Terukov, E. I.; Kudoyarova, V. Kh.; Weiser, G.; Keuhne, H. *Semiconductors* **2001**, *35*, 1263.
(17) Birdwell, A. G.; Glosser, R.; Leong, D. N.; Homewood, K. P. *J. Appl. Phys.* **2001**, *89*, 965−972.
(18) Kumar, A.; Dalapati, G. K.; Hidayat, H.; Law, F.; Tan, H. R.; Widenborg, P. I.; Hoex, B.; Tan, C. C.; Chi, D. Z.; Aberle, A. G. *RSC Adv.* **2013**, *3*, 7733−7738.
(19) Maeda, Y.; Umezawa, K.; Hayashi, Y.; Miyake, K. *Thin Solid Films* **2001**, *381*, 219−224.
(20) Terai, Y.; Maeda, Y. *Appl. Phys. Let.* **2004**, *84*, 903−905.
(21) Xu, J.; Yao, R.; Liao, R. *Phys. B* **2012**, *407*, 756−758.
(22) Terai, Y.; Hashimoto, S.; Noda, K.; Fujiwara, Y. *Phys. Status Solidi C* **2009**, *6*, 1488−1491.
(23) Li, F.; Lustig, N.; Klosowski, P.; Lannin, J. S. *Phys. Rev. B* **1990**, *41*, 10210.
(24) Kuroda, R.; Liu, Z.; Fukuzawa, Y.; Suzuki, Y.; Osamura, M.; Wang, S.; Otogawa, N.; Ootsuka, T.; Mise, T.; Hoshino, Y.; Nakayama, Y.; Tanoue, H.; Makita, Y. *Thin Solid Films* **2004**, *461*, 34−39.
(25) Oh, W. K.; Hussain, S. Q.; Lee, Y. J.; Lee, Y.; Ahn, S.; Yi, J. *Mater. Res. Bull.* **2012**, *47*, 3032−3035.
(26) Lee, S.; Tark, S. J.; Kim, C. S.; Jeong, D. Y.; Lee, J. C.; Kim, W. M.; Kim, D. *Curr. Appl. Phys.* **2013**, *13*, 836−840.